

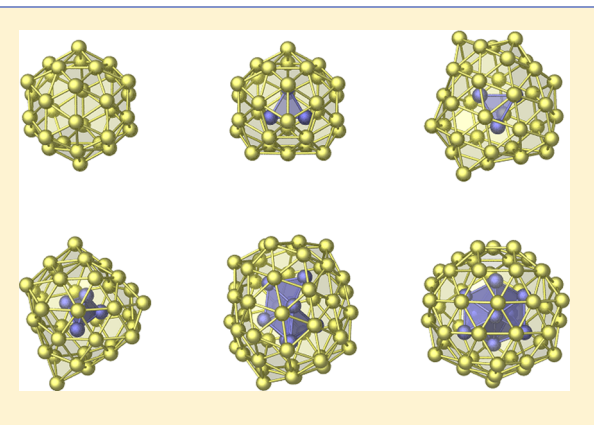
# Toward ab Initio Ground States of Gold Clusters via Neural Network Modeling

Published as part of The Journal of Physical Chemistry virtual special issue "Machine Learning in Physical Chemistry".

Aidan Thorn,\*,† Javier Rojas-Nunez,\*,† Samuel E. Baltazar,\*,† Samuel E. Baltazar,\*,† and Aleksey N. Kolmogorov\*,†

Supporting Information

ABSTRACT: Prescreening candidate structures with reliable classical potentials is an effective way to accelerate ab initio ground state searches. Given the growing popularity of machine learning force fields, surprisingly little work has been dedicated to quantifying their advantages over traditional potentials in global structure optimizations. In this study, we have developed a neural network (NN) model and systematically benchmarked it against a commonly used Gupta potential and an embedded atom model in the search for stable Au<sub>N</sub> clusters (30  $\leq N \leq$  80). An efficient simultaneous optimization of clusters in the full size range was achieved with our recently introduced multitribe evolutionary algorithm. Density functional theory (DFT) evaluations of candidate configurations identified with the three classical models revealed that the NN structures were lower in energy by at least 10 meV/atom for 30 of the 51 sizes. We also demonstrated



that DFT evaluation of all NN-relaxed structures during evolutionary searches resulted in finding even more stable configurations, which highlights the need for further improvement of the NN accuracy to avoid excessive DFT calculations. Overall, the global searches produced putative ground states with matching or lower DFT energies compared to all previously reported Au clusters with 30-80 atoms.

#### INTRODUCTION

Chemically inert crystalline gold (Au) transforms into an unexpectedly active catalyst once the material's size is reduced down to the nanoscale. 1-6 Over the past 3 decades, Au nanoparticles have been found to catalyze NO reduction, N2O decomposition, and numerous organic reactions.<sup>7</sup> One of the applications that distinguishes Au from other metals is the nanocatalytic oxidation of CO at subroom temperatures.8 Extensive research into Au clusters has indicated that their catalytic behavior is determined primarily by the activity of low-coordination atoms, 9-11 effects arising from the presence of substrates, 8,12,13 and size-dependent electronic features. These findings highlight the importance of establishing nanoparticle morphology as a function of size and operating conditions for rational design of high-performance catalysts.

The existence of an upper limit on the Au nanoparticle size to efficiently catalyze certain reactions 14-16 has prompted systematic experimental and computational studies of (ultra)small systems below 2 nm, which included neutral, 1 anionic, <sup>22-27</sup> and functionalized <sup>28-31</sup> Au clusters. Even in the simplest case of bare neutral elemental nanoparticles at zero

temperature, the N = 150-200 systems with a near 2 nm diameter, are beyond the capability of ab initio unconstrained structure prediction methods. 32-34 The computational bottleneck is the exponential growth of possible configurations with the cluster size, which necessitates the use of approximated methods to evaluate the Gibbs free energy of relevant structures.

Structure prediction and stability analysis studies for bare neutral Au nanoparticles have relied on four distinct methods of interaction description: density functional theory (DFT) approximations, density functional based tight-binding (DFTB) method, empirical potentials, and neural network (NN) models. Global structure searches with the computationally demanding DFT have been restricted to Au<sub>N</sub> clusters with diameters below ~1.2 nm, e.g., N = 9-13, N = 12-12 $14^{36}$   $N = 15-19^{37}$  and  $N = 38,40^{.38}$  The computational studies revealed that Au prefers 2D sheets over 3D

Received: September 6, 2019 Revised: November 1, 2019 Published: November 25, 2019

Department of Physics, Applied Physics and Astronomy, Binghamton University, State University of New York, PO Box 6000, Binghamton, New York 13902-6000, United States

<sup>&</sup>lt;sup>‡</sup>Department of Physics and CEDENNA, Universidad de Santiago de Chile, Av. Ecuador 3493, Santiago 9170124, Chile

configurations up to larger sizes  $(N=11-17)^{35,37,39}$  than other noble metals<sup>39</sup> and exhibits unusual morphologies for larger system sizes, such as the hollow fullerene for  $\mathrm{Au_{32}}^{40,41}$  According to electronic structure analyses, this behavior arises from the directionality of the d-orbitals and the relativistic effects causing a strong s-d orbital hybridization.<sup>42,43</sup>

The use of DFTB, empirical potentials, and NNs has considerably extended the scope of systematic unconstrained structure searches. Tarrat et al. performed DFTB-based global structure searches with a combination of replica exchange and periodic quenching for N = 20, 55, and 147 and checked the stability of best configurations with several DFT flavors. 44,45 Narayanan et al. used a modified hybrid bond-order potential to search for global minima of several small cluster sizes with N ≤ 20 and presented a comparison between their potential, a previous bond order potential, and the DFT for the cohesive energies of representative  $A_{40}$  and  $A_{75}$  configurations. <sup>46</sup> Putative ground states have been identified for  $13 \le N \le 80$ with the Sutton-Chen potential (SCP) and the basin-hopping method, <sup>47</sup> for select sizes in the  $13 \le N \le 300$  range with the Gupta potential (GP) and the dynamic lattice searching, 18,48 and for  $30 \le N \le 147$  with the GP and the basin-hopping method.<sup>17</sup> The low computational cost of the classical calculations allowed Schebarchov et al. to investigate the thermodynamic stability of select 55-, 85-, and 147-atom Au clusters at finite temperatures as well. <sup>17</sup> These studies provided important insights into the evolution of morphological features with the cluster size and ambient temperature but it has been acknowledged that the limited transferability of empirical potentials might not allow one to accurately resolve and correctly order competing configurations.<sup>17</sup> Recent introduction of machine learning NN interatomic models fitted to DFT data holds promise for a more accurate mapping of the potential energy surface (PES).<sup>49–51</sup> Unconstrained searches based on NNs have already been used to help identify ab initio ground states for Au clusters of select sizes (N = 34, 58, and147). 52-54 Yet, there is a surprising paucity of studies that compare classical interatomic description methods systematically and make a convincing case for choosing NNs over traditional potentials in global structure searches.

In this work, we have assessed the suitability of a typical NN model and popular empirical potentials for locating global minima on the DFT PES. We carried out extensive evolutionary searches with our developed NN model, a Gupta potential (GP), and an embedded atom model (EAM) for Au clusters in the  $30 \le N \le 80$  range. We employed a multitribe evolutionary algorithm introduced in our recent study<sup>55</sup> for an efficient simultaneous optimization of the entire population of clusters in the chosen size range. With our previous study's focus on benchmarking NNs against the GP for multiple chemical elements and their alloys, we ran DFT calculations to test only the best member per composition and size in the NN and GP pools.<sup>55</sup> In the present study dedicated to a single metal, we have been able to evaluate multiple metastable configurations for each Au cluster size with the DFT. The examination involved (i) full DFT relaxations of up to 60 candidate structures at the end of NN/ GP/EAM evolutionary runs for  $30 \le N \le 80$  or (ii) static DFT evaluations of each NN-relaxed structure during NN evolutionary runs for  $37 \le N \le 41$ , N = 55, and N = 58. The resulting combined set of Au configurations produced with the help of the NN has matching or improved stability compared to all previously reported structures with  $30 \le N \le 80$ . In

particular, the ground state of bare neutral Au<sub>55</sub> has been the subject of long debate <sup>17,19–21,56</sup> because it differs from the highly symmetric icosahedron adopted at this magic size by many metals. <sup>21,57,58</sup> A number of studies have concluded that Au<sub>55</sub> has amorphous morphology. <sup>19,20,44,45,59</sup> Our searches uncovered a new amorphous configuration that is more stable at the DFT level than any other candidates for which full structural information is available. <sup>17,21</sup> In addition to the Au cluster stability analysis with different interaction description methods at zero temperature, we compared the vibrational entropy contributions to the free energy at elevated temperatures for select sizes with the DFT. NN. and GP.

#### COMPUTATIONAL METHODS

**Density Functional Theory.** All DFT calculations were performed with the Vienna *ab initio* simulation package (VASP). $^{60-63}$  We used the Perdue–Burke–Ernzerhof (PBE) exchange-correlation functional $^{64}$  within the generalized gradient approximation $^{65}$  and the projector augmented wave (PAW) potential with 11 valence electrons. $^{66}$  All final static calculations were carried out with the energy cutoff of 500 eV to ensure good convergence of the relative energies and forces with respect to the plane wave basis. As in our previous study, $^{55}$  reference crystalline structures for NN training were evaluated with dense ( $\Delta k \sim 0.04 \text{ Å}^{-1}$ ) Monkhorst–Pack k-point meshes $^{67}$  and the Methfessel–Paxton 0.1 eV smearing. The same smearing method was used in the Γ-point simulation of NPs placed in 25 Å boxes. Optimization of NPs proceeded until residual forces dropped below 0.06 eV/Å.

Neural Network Model. The sampling of the configuration space and the fitting of the Au NN model was done with our MAISE<sup>68</sup> package and followed the procedure described in our previous study on similar Cu, Pd, and Ag metals.<sup>55</sup> The first stage of structure database generation involved short evolutionary runs of randomly initialized small crystalline unit cells with 1-6 atoms.<sup>69</sup> The purpose of this approach is to sample parts of the configuration space typically visited in unconstrained structure searches. We complemented this bulk data set of 3000 structures with 385 compressed/ expanded close-packed structures and short-distance dimer/ square clusters to reduce the number of artificial minima. 55,69 A preliminary "bulk" NN trained on this data showed a good performance for crystalline configurations. In order to improve the model's description of NP geometries, the second stage involved evolutions of NP populations using the bulk NN instead of DFT for short optimizations. We generated 160 cluster configurations for 16 equally spaced sizes in the 5-80 atom range. The resulting combined set comprised 3235 structures after discarding 10% of the highest energy data points. The energy versus volume distribution is shown in Figure S1.

Atomic environments within 7.5 Å radius spheres were converted into NN inputs with 51 Behler–Parinello symmetry functions  $^{50}$  (the full set of parameters and functional form of the symmetry functions are given in Tables S1 and S2). The NN had 20 neurons with the hyperbolic tangent activation function in two hidden layers, one output neuron with the linear activation function, and three standard biases. The resulting 51-10-10-1 NN had  $(51+1)\times 10+(10+1)\times 10+(10+1)=641$  adjustable parameters. We chose to use this architecture because (i) it was shown to provide a good balance between accuracy and efficiency in our previous studies  $^{55,69}$  and (ii) it allowed us to compare the NN

performance for related Cu, Pd, and Ag elements.<sup>55</sup> The weights were first tuned with the BFGS algorithm to 2,912 DFT target energies for 40 000 minimization steps, and then to the DFT energies and 21,621 force components for 50 000 steps. We also used the  $L_2$  regularization with the  $10^{-6}$  value, but its effect was insignificant due to the large data to parameter ratio. The test energy and force errors were 6.5 meV/atom and 37 meV/Å respectively, consistent with our previously reported values obtained for Cu, Pd, and Ag.55 Figure S2 gives the histograms of energy error distributions for the bulk and cluster data. Additional tests of the trained NN illustrated a reliable description of diverse environments. The equation of state curves in Figure S3 show the NN's capability to resolve bulk structures with considerably different coordinations. The low-index surface energies in fcc and bcc calculated with the bulk NN matched the DFT values to within 18%; the errors decreased further down to 10% after the cluster geometries were included in the training set (see Figure S4). Finally, Figure S5 shows a good correspondence between the NN model and the DFT in the description of vacancy formation energies in bcc, fcc, and hcp to within 11%, 18%, and 12%, respectively.

**Empirical Models.** The Gupta potential  $^{70,71}$  is a popular choice for modeling crystalline and nanosized materials with predominantly metallic bonding. Based on the second moment tight-binding approximation, this potential has a pairwise repulsive term defined by the A and p parameters and a many-body attractive term defined by  $\eta$  and q, with  $r^{(0)}$  as a scaling factor:

$$E = \sum_{i=1}^{N} \left( \sum_{j \neq i}^{N} A e^{-p(r_{ij}/r^{(0)}-1)} - \sqrt{\sum_{j \neq i}^{N} \eta^{2} e^{-q(r_{ij}/r^{(0)}-1)}} \right)$$
(1)

Among several parametrizations fitted to experimental data for Au, two have been used in recent studies of Au clusters. <sup>17,18</sup> By default, we used the set with A = 0.21 eV,  $\eta = 1.818$  eV, p = 10.35, q = 4.178, and  $r^{(0)} = 2.88$  Å. <sup>18,98</sup> We also tested the set with A = 2.197 eV,  $\eta = 1.855$  eV, p = 10.53, q = 4.30, and  $r^{(0)} = 2.88$  Å. <sup>17</sup> Select structures were assessed with the SCP, which had the  $\epsilon = 0.012793$ , a = 4.08, c = 34.408, m = 8, and n = 10 parameters fitted to DFT data. <sup>59</sup> No cutoff for nearest neighbor distances was imposed in the NP simulations. While the NN formalism, the GP, and the SCP are implemented in MAISE, we relied on the LAMMPS package <sup>76</sup> to perform simulations with the EAM. The consideration of EAM was important for the NN benchmarking because the model has a more flexible functional form than the GP and was fitted to DFT-PBE data. <sup>77</sup> The full set of the EAM parameters is given in Table S3.

**Evolutionary Searches.** Identification of most stable configurations requires application of advanced search methods even in the idealized case of free-standing elemental NPs at zero temperature. The basin-hopping method,  $^{78,79}$  particle swarm optimization,  $^{80}$  dynamical lattice searching, and evolutionary algorithms,  $^{82-84}$  among others, have proven to be efficient strategies for PES exploration but finding global minima for modest-sized NPs with 50–100 atoms still involves the consideration of  $10^4\!-\!10^5$  structures.

In an effort to accelerate the search for ground states across a range of NP sizes, we have recently developed, tested, and used a multitribe variation of the evolutionary algorithm. <sup>55</sup> The first difference from typical implementations is the introduction of

new operations for generating and evolving the structures. They include a Tetris-like creation of compact random structures, a Rubik's cube mutation, and a facet creation mutation. The main departure from the standard evolutionary algorithms is the periodic exchange of seeds among tribes of neighboring sizes followed by periods of isolated single-tribe evolutions. We argued that some morphologies, e.g., icosahedron shapes, tend to be stable over several sizes but might be found much faster for certain sizes, e.g., for N=55. Therefore, sharing seeds across populations has the benefit of a symbiotic coevolution and was shown to significantly improve the global search efficiency.  $^{55}$ 

In the multitribe evolutionary searches based on the NN, GP, or EAM for  $30 \le N \le 80$  Au clusters, populations of 100 members per size were created randomly with the Tetris-based procedure. The tribes were then evolved for 10 generations in isolation with an assortment of different operations.<sup>55</sup> Two crossover operations (based on planar or spherical cuts) produced 20 offspring and five mutation operations (Rubik's cube rotation, reflection, inversion, facet creation, and distortion) generated 50 child structures. The remaining 30 offspring were picked randomly from a pool of 51 seed structures and some surface atoms were optionally redistributed. The pools were updated every 10 generations and contained lowest-energy configurations from the current tribe (19 seeds) and from 8 tribes of neighboring sizes (32 seeds). The multitribe evolutionary runs totaled 400 generations for the GP- or EAM-based searches and 250 generations for the NN-based searches. Figure S7 shows the average energy drop of the ground state across all sizes per every tenth generation. The results indicate that the frequency and the magnitude of the energy gains become insignificant after about 200 generations.

Select  $37 \le N \le 41$  sizes were explored further with a multitribe search based on a combination of the NN and DFT methods. In this case, candidate structures were fully relaxed with the NN model but their stability (fitness) was evaluated with a static DFT calculation at medium accuracy. This adjustment makes the otherwise Lamarckian evolution partly Darwinian and helps steer the population toward low-energy regions of the DFT PES. Due to a roughly 10-fold increased cost of this hybrid NN+DFT approach, which remains about 2 orders of magnitude lower than the cost of pure DFT searches for clusters of such sizes, we limited the runs to 360 generations of 50 members. For comparison, we also investigated N=55 and 58 with a single-tribe NN+DFT evolutionary search.

**Selection of Candidate Structures.** Coarse-graining complex PES's leads to inevitable mismatches in the number, location, and ordering of competing minima. With the expectation that the true global minimum is at least a local minimum visited in the exploration of low-energy regions of the approximated PES, select configurations are commonly reoptimized with more accurate DFT-level methods. <sup>17,85</sup> The choice of relevant candidate NP structures is not straightforward because of the large number of similar-energy local minima corresponding to minor variations in the positions of surface atoms. In order to reduce the number of structures from the same basin, we imposed a 0.98 cutoff on their similarity, calculated as a scalar product between two structures based on the radial distribution function (RDF). <sup>86</sup>

Figure 1 illustrates the distribution and reordering of energies in the NN and GP pools, which included lowest-

The Journal of Physical Chemistry C

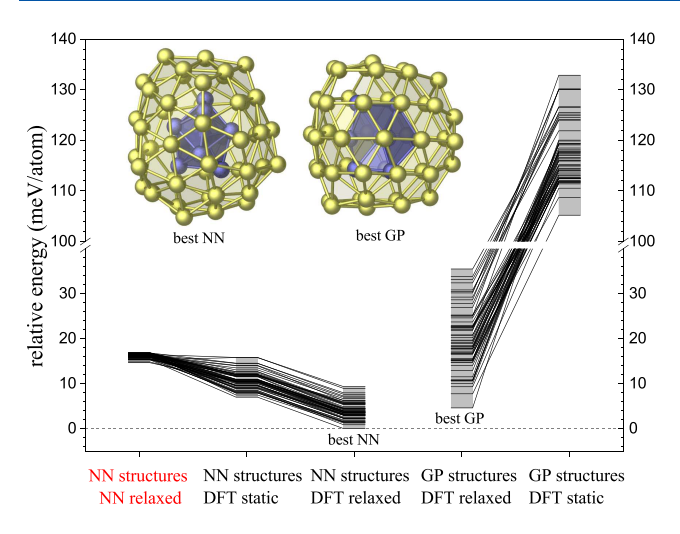


**Figure 1.** Relative energies of 60 best 55-atom clusters found with NN- and GP-based evolutionary searches and chosen with the 0.98 similarity cutoff as described in the main text. The zero level is set to the DFT energy of the best structure reoptimized at the DFT level. The leftmost box displays NN energies, while all other sets are DFT energies. The GP energies cannot be compared directly with the DFT and are not shown.

energy structures with no more than 0.98 similarity. For the NN set of 60 55-atom configurations, the NN energy range of 2.2 meV/atom expanded to 8.8 meV/atom once the clusters were evaluated at the DFT level. The size of the energy dispersion and the degree of reordering are consistent with the NN's 6.5 meV/atom accuracy and demonstrate why a large number of candidate structures should be examined. However, subsequent structural reoptimization with DFT had a minor effect on the energy range and the candidates' ranking. Figure 2 shows that the DFT-level relaxation disperses the energies of NN local minima for all sizes by a comparable 15 meV/atom. On the basis of these observations, the number of viable

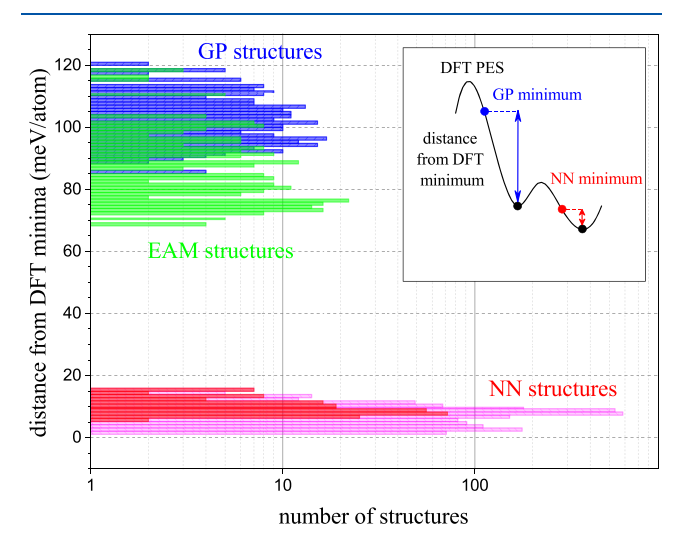


**Figure 2.** Histogram of energy gains in the DFT reoptimization of Au clusters found in global searches with the NN, GP, and EAM using the pool of 5 structures from each search. The inset is a schematic illustration of typical DFT energy differences between starting configurations relaxed with the NN or GP and final configurations relaxed with the DFT. The magenta data set represents the pool of 60 structures from the NN search.

candidates needed to be reoptimized at the DFT level could be reduced with less expensive static DFT evaluations.

In contrast, the 3.4 meV/atom energy range for structures in the GP pool expanded to 27.7 meV/atom at the DFT level and showed a high degree or reordering in subsequent DFT reoptimization runs. Results in Figure 2 indicate that both GP and EAM minima are far away from the corresponding DFT minima. Therefore, many more structures in the GP/EAM pools would need to be relaxed with DFT to determine ab initio ground states. Since the EAM and NN were fitted to the same flavor of the DFT, the difference in the performance between the traditional potentials and the NN can be attributed to the functional forms rather than the training data. As detailed in the Results and Discussion, the benchmarking of the three classical potentials across all NP sizes was done with 5 dissimilar lowest-energy structures from each pool. In select cases, up to 60 candidate configurations were examined at the DFT level.

**Thermal Corrections.** Evaluation of vibrational entropy corrections to the free energy at elevated temperatures for select structures was done with the PHON package. <sup>87</sup> We chose the finite displacement method because it can be used for both the DFT and classical potential levels of interaction description. We found that the 0.1 Å displacement provided well converged phonon density of states results.

Morphology Classification. Identification of point group symmetry for relevant structures was done with the SYMMOL package using a 0.01 Å tolerance. To check whether the fully optimized clusters represented slightly distorted versions of more symmetric motifs, we repeated the analysis with a much higher tolerance of 0.7 Å and found that only 2 out of 204 considered structures gained additional symmetries. Categorization of atoms into core or surface types based on their local environments provides useful information about the morphology of small clusters. We relied on the centrosymmetry analysis implemented in the OVITO software <sup>89,90</sup> and classified atoms as core if they had the centrosymmetry parameter below 17 Å<sup>2</sup> considering 12 nearest neighbors.

# ■ RESULTS AND DISCUSSION

Searches with Different Interatomic Potentials. We started the investigation of Au stable motifs with GP-based multitribe evolutionary searches. The global optimization of 30  $\leq N \leq$  80 clusters allowed us to systematically test the performance of our approach against the dynamic lattice searching method. 18 We observed that the most stable structures found within 400 generations had either matching or lower GP energies compared to the previously published putative ground states. 18 The five improved sizes of N = 50, 60, 61, 74, and 79 were up to 1.1 meV/atom more stable at the GP level. For evaluation of different GP parametrizations, we reoptimized the best structures reported in two previous studies<sup>17,18</sup> with VASP. The set from the more recent study<sup>17</sup> was found to have lower DFT energies by 1.7 meV/atom on average, with the majority of the relative energies within 1 meV/atom.

Having obtained further supporting data on the reliability of the coevolutionary algorithm, we carried out ground state searches with the EAM and the NN for 400 and 250 generations, respectively. The runs with the three classical models produced between 1000 and 3000 nonidentical metastable structures within 10 meV/atom above the ground state for some sizes. Using the selection procedure described in

Selection of Candidate Structures, we collected five lowestenergy structures per size for each interatomic potential and reoptimized the combined set of 765 configurations with the DFT to determine which classical description provided the closest mapping of the DFT PES.

Figure 3 shows the lowest DFT energies in each fivestructure set (half-filled symbols) referenced to the GP-pool

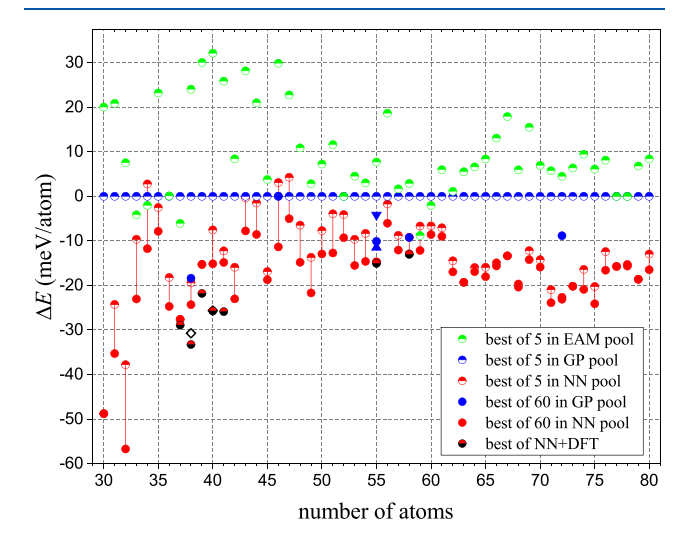


**Figure 3.** Relative stability of DFT-optimized structures selected from our GP, EAM, and NN pools (circles) or previous studies (other shapes). The semifilled (solid) circles correspond to sets with 5 (60) members. The half-red half-black circles show the energies for best 37  $\leq N \leq 41$ , N=55, and N=58 configurations obtained with the hybrid NN+DFT search. The triangle, inverted triangle, and hollow diamond denote clusters with lowest DFT energies proposed by Piotrowski et al., <sup>21</sup> Schebarchov et al., <sup>17</sup> and Jiang and Walter, <sup>38</sup> respectively. Values for each cluster size are referenced to the lowest DFT energy in the corresponding GP five-member set.

values. The results reveal that practically none of the starting configurations from the three GP, EAM, and NN pools converged to the same lowest-energy DFT minima, with the exception of N=36, 52, 77, and 78 for the traditional potentials. To quantify the overall agreement between the DFT and classical representations of the PES, we averaged the differences between the best-of-5 DFT energies over all sizes for the three models. On average, the DFT minima originating from the EAM (GP) structures were found to be 22.8 (13.2) meV/atom higher in energy compared to those from the NN set. For the 51 considered sizes, 3, 2, and 46 lowest DFT minima were obtained from the GP, EAM, and NN sets, respectively.

The findings presented in Figures 1–3 illustrate clear advantages of the NN over the considered traditional potentials to guide *ab initio* ground state searches. We extracted 55 more metastable configurations per size from the NN pool for further DFT analysis. Compared to the five-member subsets, the consideration of additional candidates improved the cluster stability for 42 out of 51 sizes and lowered the average energy of the resulting DFT minima by 4.5 meV/atom. As in the case of the 55-atom clusters discussed in the Introduction, the NN energies in the 60-member pools dispersed by only 2–6 meV/atom for each size. Considering that the NN energy ranges remained smaller than the NN error, it is not surprising that the putative DFT ground states were found to be deep in the collected populations for most

cluster sizes. For a more reliable identification of *ab initio* global minima, the number of selected candidates should be increased further to ensure that the NN energy range noticeably exceeds the model's typical errors. Since the density of metastable states tends to grow with energy, the pools may become too large for DFT evaluations. These arguments highlight the importance of using classical models with low energy and force errors to reduce the number of candidates and the length of relaxations. For comparison, we expanded the GP sets to 60 configurations for five select sizes of 38, 46, 55, 58, and 72. The best DFT minima derived from these configurations dropped by 9.3 meV/atom in energy on average but remained above the NN-based DFT minima (see Figure 3). Images of best NN and DFT minima for each size are assembled in Tables S4 and S5.

The results of the additional NN+DFT multitribe optimization for  $37 \le N \le 41$  and the single-tribe searches for N=55 and 58 demonstrate the remaining limitations of the empirical and machine learning models. The course correction in the exploration of the PES accomplished with regular DFT evaluations of NN-relaxed structures helped the populations locate noticeably better DFT minima in six of the seven considered cases. Subsequent high-accuracy DFT relaxations of the five best candidates showed very little variation in the energy gain, which kept the lowest-energy candidates best for four out of the seven considered sizes. The resulting putative ground states turned out to be 0.3 to 11.0 meV/atom more stable compared to the corresponding NN-based structures (see Figure 3 and Table 1). We note that the use of the NN

Table 1. Putative Ground States Found in the Hybrid NN +DFT Evolutionary Searches<sup>a</sup>

size	point group	core atoms	$\Delta E$ (meV/atom)
37	$C_s$	3	-1.3
38	$C_1$	3	-9.0
39	$C_1$	3	-6.5
40	$C_3$	3	-10.6
41	$C_3$	4	-11.0
55	$C_1$	8	-0.3
58	$C_s$	11	0.0

<sup>a</sup>DFT energy differences  $\Delta E$  represent the improvements over the best structures from our NN-based searches.

model in these hybrid searches was crucial because the GP/EAM-relaxed structures are too far away from the corresponding DFT minima to give an accurate assessment of the DFT minima energies.

Comparison of Previous and Proposed Structures. In order to assess the soundness of the NN-guided predictions, we checked our putative ground states against previously proposed structures. The use of the same PAW-PBE approximation in the relevant published studies on Au clusters 17,21,38,52,53 simplified the comparison. We did test the sensitivity of the results to other DFT settings, such as the energy cutoff and the box size, by performing calculations with both "reference" and "current" parameters specified in Table 2.

The ground state morphology of Au<sub>32</sub> proposed by Johanssen et al.<sup>40</sup> and shown in Figure 4 is a fitting illustration of the noble metal's unusual preference for directional bonding. Our evaluation of 60 competing structures from the NN pool supports the view that the 32-atom fullerene has the lowest DFT energy. At the NN level, the hollow structure was

Table 2. Relative Energies ( $\Delta E$ ) in meV/atom of our Putative Ground States Referenced to Previously Reported Structures<sup>a</sup>

size	point group	study	interaction description	search method	reference DFT settings	$\Delta E \; ({ m meV/atom})$ reference DFT	$\Delta E \; (\text{meV/atom}) \; \; \; \; \; \; \; \; \; \; \; \; \; \; \; \; \; \; \;$
32	$I_h$	Johannsen et al. <sup>40</sup>	DFT	predefined structure	not specified	0.0	0.0
34	$C_s$	Chiriki et al. <sup>52</sup>	NN and DFT	basin-hopping	250 eV and 25 Å	-0.1	-0.1
38	$C_2$	Jiang and Walter <sup>38</sup>	DFT	basin-hopping	not specified	-2.6	-2.6
40	$C_3$	Jiang and Walter <sup>38</sup>	DFT	basin-hopping	not specified	0.0	0.0
55	$C_1$	Piotrowski et al. <sup>21</sup>	DFT	predefined structures	240 eV and 22 Å	-3.5	-3.6
55	$C_s$	Schebarchov et al. 17	GP and DFT	basin-hopping	544 eV and 29 Å	-10.9	-10.9
58	$C_4$	Chiriki et al. <sup>52</sup>	NN and DFT	basin-hopping	250 eV and 25 Å	-2.9	-0.2
58	$C_4$	Ouyang et al. <sup>53</sup>	NN and DFT	basin-hopping	500 eV and 25 Å	0.0	0.0

"Energy evaluations were performed using two sets of plane wave cutoff energy and box size: one set to match the settings used in the corresponding published study and another at our settings of 500 eV cutoff and 25 Å box size. For N = 32 and 40, we reproduced previously proposed ground states. For N = 58, we found a new structure with virtually identical energy  $|\Delta E| < 0.02$  meV/atom compared to the best known one.

ranked ninth in the pool and ended up 2.0 meV/atom above a more conventional compact configuration. At the GP level, the fullerene is unstable by 122 meV/atom above the perceived GP ground state. It is evidently kept from collapsing by the structure's high symmetry because less symmetric "bubbles" with 30-32 atoms that represent local minima on the DFT and NN PES readily transformed into dense clusters upon local relaxation with the GP. We repeated the reoptimizations with the SCP fitted to DFT data and observed a similarly large energy gap of 127 meV/atom between the fullerene and the GP ground state. The finding is consistent with our observation that these potentials considerably overestimate vacancy formation energies (Figure S5). We performed additional tests to evaluate energies required to remove atoms from small 1D-3D clusters (Figure S6). We observed that the GP and EAM overestimate the energies by 54% to 85% compared to the DFT, while the NN generally agrees with the DFT to within 14%. This test case illustrates again that traditional potentials with different but fixed functional forms display common limitations with little dependence on the reference data used to fit the few adjustable parameters.

The search for Au ground states with 34 atoms by Chiriki et al. serves as a good reference because the authors also relied on a NN model and examined the resulting configurations with the DFT. They evaluated several low-lying Au<sub>34</sub> isomers with 2–4 atom cores found with the basin-hopping method. The previously reported and our lowest-energy structures differ only in the orientation of the three-atom core unit. Our putative ground state has a mirror plane symmetry, and each core atom resides near the bottom of a pentagonal pyramid. This placement of the core triangle has a small but reproducible favorability of about 0.1 meV/atom at different DFT settings (Table 2).

Unconstrained optimization of Au<sub>38</sub> and Au<sub>40</sub> directly with the DFT allowed Jiang and Walter<sup>38</sup> to uncover interesting stable morphologies shown in Figure 4. For size 40, the authors identified related 3- (Jia40b) and 4-core (Jia40a) chiral pyramid configurations and determined the latter to be more stable by 3.8 meV/atom. Our  $37 \le N \le 41$  searches produced both structures but our DFT calculations favored the three-core allotrope by 0.6 meV/atom (see Figure 3 and Table 1). These configurations can be derived from a perfect 41-atom pyramid with a triangular base by removing the top atom from the 4-atom core or an atom from one of the three corners. In fact, our examination of the motif propagation in the multitribe

search revealed that the 41-atom ground state was determined first and then the seed exchange operation generated competitive derivatives for the smaller sizes. The 40-atom pyramids, especially the one with the 3-atom core, were not favored by any of the considered classical models. Namely, Jia40b was 20.0, 33.2, and 57.7 meV/atom less stable than the corresponding NN, GP, and EAM ground states evaluated with the respective classical models. The only reason the structure was somewhat competitive in the GP and EAM treatments is because the pyramid caved in to fill the void above the threeatom core unit. Compared to the previously proposed Au<sub>38</sub> with a four-atom core, 38 we found a more stable configuration (by 1.5 meV/atom) ranked 133rd in our extended NN pool and an even more favorable (by 2.6 meV/atom) three-atom core configuration in the NN+DFT search after DFT reoptimizations.

For size 55, Piotrowski et al.<sup>21</sup> used 25–40 existing atomic configuration templates and found a structure with  $C_1$  point group symmetry to have the lowest DFT energy, evaluated with a plane wave cutoff of 240 eV and a box size of 22 Å. Ranked fifth in our NN pool and 0.7 meV/atom above the NN ground state, a different C<sub>s</sub> structure had a noticeably lower DFT energy of  $\sim 3.2 \text{ meV/atom}$  with either choice of the DFT settings. Schebarchov et al. specified 16 best GP-based minima and determined a  $C_s$  structure among them to have the lowest energy at the DFT level. Compared to our proposed  $C_s$ configuration, the Sch55 isomer is unstable by 10.5 meV/ atom. As shown in Figures 1 and 3, the extension of the GP pool to 60 configurations allowed us to reduce the gap down to 4.6 meV/atom. Our separate NN+DFT evolutionary run uncovered an even more favorable amorphous structure, 0.3 meV/atom below the lowest-energy cluster in the NN pool.

For Au<sub>58</sub>, NN-based basin-hopping searches have been carried out by two groups. <sup>52,53</sup> Interestingly, the two previous and our current studies produced three different competing DFT minima within ~0.1 meV/atom from each other. <sup>99</sup> By inspecting the full set of metastable structures we found that neither Chi58 ( $C_4$ ) nor Ouy58 ( $C_4$ ) was encountered in our NN search, which converged to NN58 ( $C_s$ ). This result illustrates the difficulty of establishing the specific most stable shape for even modest-sized clusters with amorphous morphology. The best DFT minimum in the GP pool of 60 candidates remained 1.3 meV/atom above NN58, while the NN+DFT run converged to the same NN58 structure.

The Journal of Physical Chemistry C

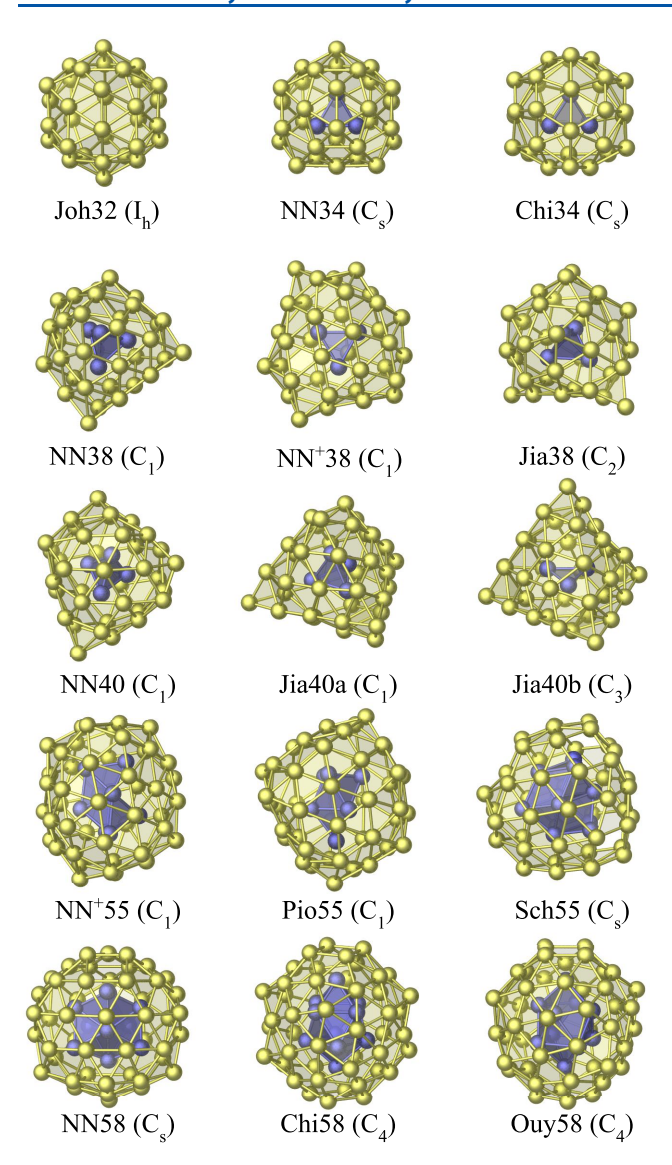


**Figure 4.** Illustration of core (yellow) and shell (blue) atoms in low-energy Au clusters. Putative ground states found in our NN and NN +DFT searches are denoted as NN and NN<sup>+</sup>, respectively. The previously proposed low-energy structures are labeled using the first author's name as follows: Joh32, <sup>40</sup> Chi34 and Chi58, <sup>52</sup> Jia38, Jia40a, and Jia40b, <sup>38</sup> Pio55, <sup>21</sup> Sch55, <sup>17</sup> and Ouy58. <sup>53</sup> Our NN searches reproduced the Joh32 hollow fullerene, and our NN+DFT searches identified both Jia40a and Jia40b pyramids.

Thermal Corrections. Analysis of NP structure stability in realistic conditions must involve a proper evaluation of the Gibbs free energy. Studies of Au NP stability at elevated temperatures have included Monte Carlo sampling at the SCP level, molecular dynamics with the GP, and harmonic superposition analysis with the GP. Results in our previous sections indicate that the traditional potentials have large errors for relative energies, which affects the estimates of the configurational entropy through the Boltzmann factors. The purpose of the following tests is to show how the vibrational entropy corrections are described with the classical potentials and the DFT.

Figure 5 summarizes the relative free energy corrections due to the vibrational entropy for select Au clusters evaluated with different interaction methods. For each considered size, we calculated relative vibrational entropy contributions as a

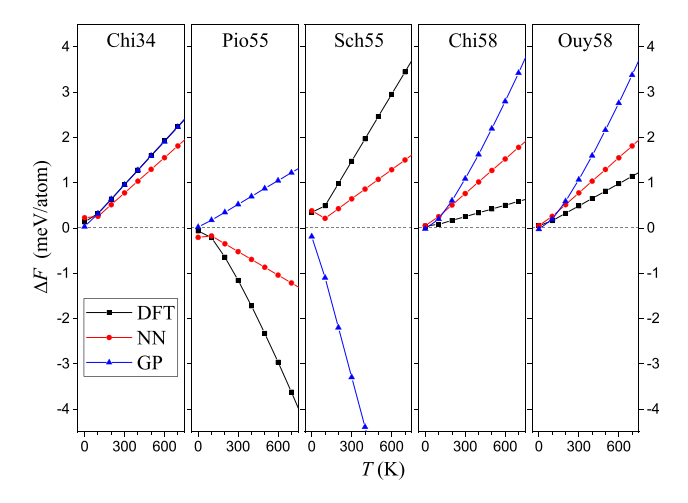


**Figure 5.** Thermal correction to the energies of NN-acquired putative ground states of various sizes relative to other published structures. Structure notation follows the abbreviations given in Figure 4.

function of temperature for known and our Au configurations. The negative values signify additional stabilization of our proposed structures, which happens for the Pio55 and NN55 pair in the DFT/NN treatment. The positive DFT corrections for the Chi34 and NN34 and Sch55 and NN55 pairs do not make our proposed structures unstable in the considered temperature range because at  $T=0~\rm K$  NN34 and NN55 were lower in energy by 6.3 and 10.5 meV/atom, respectively. For Au<sub>58</sub>, the corrections break the degeneracy of DFT energies by less than 0.5 meV/atom at a typical synthesis temperature of 300 K  $^{92-95}$  in favor of Chi58 and Ouy58. When averaged over all considered structures, the NN (GP) agreed with the DFT values to within 0.6 (2.5) meV/atom at this temperature.

These findings illustrate that while the calculated relative vibrational entropy corrections appear to be a minor factor at room temperature, not exceeding 1.5 meV/atom at the DFT level, they can be misevaluated significantly with traditional potentials. With the exception of N=34, the GP was in quantitative (N=58) or qualitative (N=55) disagreement with the DFT. The NN correctly predicted the sign of the corrections and described the magnitude within a factor of about 2 relative to the DFT results. The test set was fairly small due to the high cost of the DFT phonon calculations, but it supports the use of the NN models over the GP for modeling of NP stability at finite temperatures.

Stability and Morphology Comparison. Figure 6 compares the relative stability and morphology of Au structures favored in the NN and DFT treatments. The top panel illustrates the NN energy differences between the putative NN and DFT ground states. This information helps estimate the minimum NN energy range in which metastable structures need to be examined to find stable DFT configurations. The bottom panel shows significantly higher energy differences after the corresponding configurations were relaxed and compared at the DFT level (note the factor of 5 difference in the *y*-axis scale). Except for  $30 \le N \le 32$ , the level of agreement between the NN and DFT values is consistent with the NN accuracy (note that the error doubles in the calculation of relative energies). As discussed in the previous sections, the discrepancy for the smallest considered clusters originates from the underestimation of the hollow motif stability in all classical descriptions examined in this study.

The Journal of Physical Chemistry C

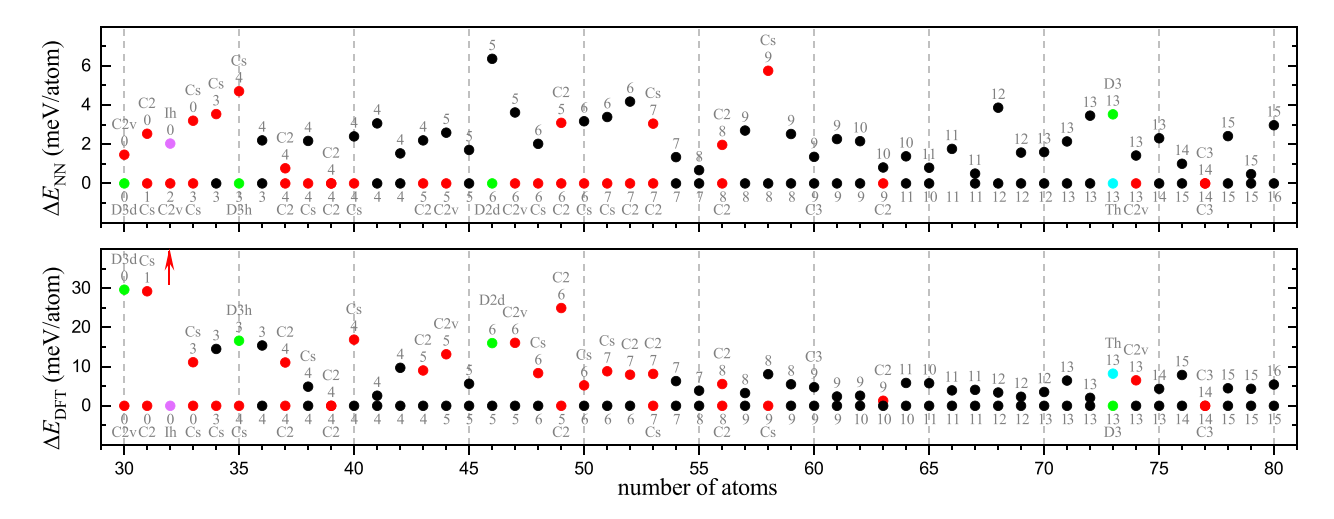


Figure 6. Relative stability of clusters found in the NN-based searches to have the lowest NN energy and the lowest DFT energy in the pool of 60. The structures were optimized at the NN (top) or DFT (bottom) level. The symbol colors specify the family of the point group symmetry: cyclic (red), dihedral (green), tetrahedral (cyan), icosahedral (magenta), and nonsymmetric (black). The number near each data point specifies the number of core atoms in the cluster. The Au<sub>32</sub> NN ground state was found to be disfavored by 56 meV/atom at the DFT level.

Overall, it is satisfying to observe that neither the symmetry nor the number of core atoms changed during the NN reoptimization (the nonzero-energy points in the top panel) of the DFT best clusters (the zero-energy points in the bottom panel) or vice versa. The NN model exhibited a higher tendency to favor symmetric structures (for 24 out of 51 sizes) compared to the DFT (for 14 out of 51 sizes). Starting with N = 34, the number of core atoms was found to be either the same for 31 sizes or different by only one.

## CONCLUSION

The primary aim of this study was to establish whether interatomic models based on NNs offer appreciable advantages over traditional potentials in guiding the search for *ab initio* ground states. We carried out multitribe evolutionary searches with our NN, a GP, and an EAM to create pools of potential global minima for neutral Au<sub>N</sub> clusters with  $30 \le N \le 80$ . By examining the five best configurations per size from each pool, we determined that the NN structures were more stable at the DFT level in 90% of cases and were favored by more than 10 meV/atom for 59% of the considered sizes (Figure 3). For five select cluster sizes, we also compared the energies of best DFT minima from extended 60-member NN and GP pools and found the NN-based minima to be more stable.

One of the GP/EAM limitations for describing small Au clusters was traced to the traditional potentials' overestimation of vacancy formation energies (Figures S5 and S6) and, consequently, an overstabilization of compact structures over cage morphologies favored in the DFT. The considerable relaxation and reordering of GP/EAM-optimized configurations at the DFT level (Figures 1 and 2) make the list of viable ab initio ground state candidates unmanageably long. The considered NN pools contained minima with matching or lower DFT energies compared to all previously reported 30 ≤  $N \leq 80$  Au structures found with the help of classical potentials. Our examination of the vibrational entropy corrections to relative free energies demonstrated a similarly better performance of the NN, as the GP was found to be in a qualitative disagreement with the DFT in some cases. The findings illustrate the importance of developing and using interaction models that can accurately describe high-temperature effects in computationally demanding simulations of nanosized systems.

Despite the encouragingly better mapping of the DFT PES achieved with the NN model, the typical accuracy of 6.5 meV/ atom for energies and 37 meV/Å for forces has been shown here to be not yet sufficient to reliably resolve the ground state morphologies in the vast configuration space of cluster geometries. For example, the most stable Au<sub>38</sub> and Au<sub>40</sub> shapes determined previously with global DFT searches proved to be considerably more stable than any of the 60 candidates obtained in our NN-based searches. The reliability can be improved by extending the pool size, as we found a more stable Au<sub>38</sub> configuration among 133 best NN structures. Moreover, a NN+DFT optimization performed at a fraction of a full DFT search cost reproduced the most stable 40-atom pyramid and uncovered a Au<sub>38</sub> structure with energy lower by 2.6 meV/atom. For the widely studied neutral Au<sub>55</sub>, both NN and NN+DFT searches identified structures more stable than any other candidates for which full structural information is available: our putative ground state is favored by 10.9 meV/atom compared to structures found previously with the GP, <sup>17</sup> by 4.9 meV/atom over the best structure in our GP 60-member pool, and by 3.6 meV/atom relative to the configuration identified directly with the DFT.<sup>23</sup>

A previous comparison of SCP parametrizations,<sup>59</sup> our benchmarking of a GP against different DFT flavors,<sup>55</sup> and the present consideration of the GP and EAM fitted to experimental and DFT data, respectively, indicate that the disagreement between these classical potentials and the DFT results predominantly from the use of rigid functional forms rather than the choice of the training data. With the continuing progress in the development of flexible machine learning interatomic models,<sup>96</sup> these new-generation interaction description methods present an attractive alternative to the traditional potentials to accelerate the search for stable materials.

## ASSOCIATED CONTENT

#### S Supporting Information

The Supporting Information is available free of charge at https://pubs.acs.org/doi/10.1021/acs.jpcc.9b08517.

DFT-PBE energy vs volume, histograms of NN errors and distributions of DFT-PBE energies, equation of state for select structures, surface energy in bcc and fcc structures, vacancy formation energy in bcc, fcc, and hcp structures, bond energy in select 2D and 3D structures, convergence of multitribe evolutionary searches, parameters used in radial and angular Behler–Parinello symmetry functions, Functional form of Behler–Parinello symmetry functions, parameters of the embedded atom model, and lowest-energy NN and DFT-PBE  $Au_N$  structures (PDF)

DFTstr.txt: Coordinate information on best structure of a 60-candidate pool of each size from pure NN evolutionary search. (TXT)

NNstr.txt: Coordinate information on best structure of a single-candidate pool of each size from pure NN evolutionary search. (TXT)

GPstr.txt: Coordinate information on best structure of a single-candidate pool of each size from Gupta potential evolutionary search. (TXT)

GPBest5str.txt: Coordinate information on best structure of a 5-candidate pool of each size from Gupta potential evolutionary search. (TXT)

Hybridstr.txt: Coordinate information on best structure of each size from hybrid NN+DFT evolutionary search. (TXT)

## AUTHOR INFORMATION

#### **Corresponding Authors**

- \*(A.T.) E-mail: athorn1@binghamton.edu.
- \*(J.R.-N.) E-mail: javes.ronu@gmail.com.
- \*(S.H.) E-mail: shajina1@binghamton.edu.
- \*(S.E.B.) E-mail: samuel.baltazar@usach.cl.
- \*(A.N.K.) E-mail: kolmogorov@binghamton.edu.

## ORCID ®

Aidan Thorn: 0000-0001-8949-4673 Javier Rojas-Nunez: 0000-0002-2343-3533 Samuel E. Baltazar: 0000-0001-9826-9400

#### Notes

The authors declare no competing financial interest.

## ACKNOWLEDGMENTS

This work used the Extreme Science and Engineering Discovery Environment (XSEDE),<sup>97</sup> which is supported by National Science Foundation Grant Number ACI-1548562. A.T., S.H., and A.N.K. acknowledge the NSF support (Award No. DMR-1821815). J.R.-N. and S.B. acknowledge DICYT Project 041931BR, USA1799 Vridei 041931SB\_GO, and the Basal Funding for Scientific and Technological Centers under Project FB0807.

# **■ REFERENCES**

- (1) Haruta, M.; Kobayashi, T.; Sano, H.; Yamada, N. Novel Gold Catalysts for the Oxidation of Carbon Monoxide at a Temperature far Below 0° C. Chem. Lett. 1987, 16, 405–408.
- (2) Hammer, B.; Norskov, J. K. Why gold is the noblest of all the metals. *Nature* 1995, 376, 238–240.
- (3) Haruta, M. Novel catalysis of gold deposited on metal oxides. *Catal. Surv. Jpn.* **1997**, *1*, 61–73.
- (4) Sanchez, A.; Abbet, S.; Heiz, U.; Schneider, W.; Häkkinen, H.; Barnett, R.; Landman, U. When Gold Is Not Noble: Nanoscale Gold Catalysts. *J. Phys. Chem. A* **1999**, *103*, 9573–9578.

- (5) Daniel, M.-C.; Astruc, D. Gold Nanoparticles: Assembly, Supramolecular Chemistry, Quantum-Size-Related Properties, and Applications toward Biology, Catalysis, and Nanotechnology. *Chem. Rev.* **2004**, *104*, 293–346.
- (6) Turner, M.; Golovko, V. B.; Vaughan, O. P. H.; Abdulkin, P.; Berenguer-Murcia, A.; Tikhov, M. S.; Johnson, B. F. G.; Lambert, R. M. Selective oxidation with dioxygen by gold nanoparticle catalysts derived from 55-atom clusters. *Nature* **2008**, *454*, 981–983.
- (7) Haruta, M. Gold as a novel catalyst in the 21st century: Preparation, working mechanism and applications. *Gold Bulletin* **2004**, 37, 27–36.
- (8) Janssens, T. V. W.; Clausen, B. S.; Hvolbæk, B.; Falsig, H.; Christensen, C. H.; Bligaard, T.; Nørskov, J. K. Insights into the reactivity of supported Au nanoparticles: combining theory and experiments. *Top. Catal.* 2007, 44, 15.
- (9) Grunwaldt, J.-D.; Maciejewski, M.; Becker, O. S.; Fabrizioli, P.; Baiker, A. Comparative Study of Au/TiO2 and Au/ZrO2 Catalysts for Low-Temperature CO Oxidation. *J. Catal.* **1999**, *186*, 458–469.
- (10) Lopez, N.; Nørskov, J.; Janssens, T.; Carlsson, A.; Puig-Molina, A.; Clausen, B.; Grunwaldt, J.-D. The adhesion and shape of nanosized Au particles in a Au/TiO2 catalyst. *J. Catal.* **2004**, 225, 86–94
- (11) Lopez, N.; Nørskov, J. K. Theoretical study of the Au/TiO <sub>2</sub>(1 1 0) interface. *Surf. Sci.* **2002**, *515*, 175–186.
- (12) van Bokhoven, J. A.; Louis, C.; Miller, J. T.; Tromp, M.; Safonova, O. V.; Glatzel, P. Activation of Oxygen on Gold/Alumina Catalysts: In Situ High-Energy-Resolution Fluorescence and Time-Resolved X-ray Spectroscopy. *Angew. Chem., Int. Ed.* **2006**, *45*, 4651–4654.
- (13) Ricci, D.; Bongiorno, A.; Pacchioni, G.; Landman, U. Bonding Trends and Dimensionality Crossover of Gold Nanoclusters on Metal-Supported MgO Thin Films. *Phys. Rev. Lett.* **2006**, *97*, 036106.
- (14) Haruta, M. Size- and support-dependency in the catalysis of gold. *Catal. Today* **1997**, *36*, 153–166.
- (15) Li, H.; Li, L.; Pedersen, A.; Gao, Y.; Khetrapal, N.; Jónsson, H.; Zeng, X. C. Magic-Number Gold Nanoclusters with Diameters from 1 to 3.5 nm: Relative Stability and Catalytic Activity for CO Oxidation. *Nano Lett.* **2015**, *15*, 682–688.
- (16) Liu, J.-X.; Filot, I. A. W.; Su, Y.; Zijlstra, B.; Hensen, E. J. M. Optimum Particle Size for Gold-Catalyzed CO Oxidation. *J. Phys. Chem. C* 2018, 122, 8327–8340.
- (17) Schebarchov, D.; Baletto, F.; Wales, D. J. Structure, thermodynamics, and rearrangement mechanisms in gold clusters—insights from the energy landscapes framework. *Nanoscale* **2018**, *10*, 2004–2016.
- (18) Wu, X.; Sun, Y. Stable structures and potential energy surface of the metallic clusters: Ni, Cu, Ag, Au, Pd, and Pt. *J. Nanopart. Res.* **2017**, *19*, 201.
- (19) Garzón, I. L.; Posada-Amarillas, A. Structural and vibrational analysis of amorphous Au<sub>55</sub> clusters. *Phys. Rev. B: Condens. Matter Mater. Phys.* **1996**, *54*, 11796–11802.
- (20) Garzón, I. L.; Michaelian, K.; Beltrán, M. R.; Posada-Amarillas, A.; Ordejón, P.; Artacho, E.; Sánchez-Portal, D.; Soler, J. M. Lowest Energy Structures of Gold Nanoclusters. *Phys. Rev. Lett.* **1998**, *81*, 1600–1603
- (21) Piotrowski, M. J.; Ungureanu, C. G.; Tereshchuk, P.; Batista, K. E. A.; Chaves, A. S.; Guedes-Sobrinho, D.; Da Silva, J. L. F. Theoretical Study of the Structural, Energetic, and Electronic Properties of 55-Atom Metal Nanoclusters: A DFT Investigation within van der Waals Corrections, Spin—Orbit Coupling, and PBE+U of 42 Metal Systems. *J. Phys. Chem. C* **2016**, *120*, 28844—28856.
- (22) Häkkinen, H.; Moseler, M.; Kostko, O.; Morgner, N.; Hoffmann, M. A.; v. Issendorff, B. Symmetry and Electronic Structure of Noble-Metal Nanoparticles and the Role of Relativity. *Phys. Rev. Lett.* **2004**, 93, 093401.
- (23) Lechtken, A.; Schooss, D.; Stairs, J. R.; Blom, M.; Furche, F.; Morgner, N.; Kostko, O.; von Issendorff, B.; Kappes, M. M. Au34-: A Chiral Gold Cluster? *Angew. Chem., Int. Ed.* **2007**, *46*, 2944–2948.

- (24) Shao, N.; Huang, W.; Mei, W.-N.; Wang, L. S.; Wu, Q.; Zeng, X. C. Structural Evolution of Medium-Sized Gold Clusters Aun— (n = 36, 37, 38): Appearance of Bulk-Like Face Centered Cubic Fragment. *J. Phys. Chem. C* **2014**, *118*, 6887—6892.
- (25) Pande, S.; Huang, W.; Shao, N.; Wang, L.-M.; Khetrapal, N.; Mei, W.-N.; Jian, T.; Wang, L.-S.; Zeng, X. C. Structural Evolution of Core—Shell Gold Nanoclusters: Aun— (n = 42–50). *ACS Nano* **2016**, *10*, 10013–10022.
- (26) Khetrapal, N. S.; Bulusu, S. S.; Zeng, X. C. Structural Evolution of Gold Clusters Aun- (n = 21-25) Revisited. *J. Phys. Chem. A* **2017**, 121, 2466-2474.
- (27) Pande, S.; Gong, X.; Wang, L.-S.; Zeng, X. C. Au60-: The Smallest Gold Cluster with the High-Symmetry Icosahedral Core Au13. *J. Phys. Chem. Lett.* **2019**, *10*, 1820–1827.
- (28) Schmid, G.; Pfeil, R.; Boese, R.; Bandermann, F.; Meyer, S.; Calis, G. H. M.; van der Velden, J. W. A. Au55[P(C6H5)3]12CI6 ein Goldcluster ungewöhnlicher Größe. *Chem. Ber.* **1981**, *114*, 3634–3642.
- (29) Pei, Y.; Shao, N.; Gao, Y.; Zeng, X. C. Investigating Active Site of Gold Nanoparticle Au55(PPh3)12Cl6 in Selective Oxidation. *ACS Nano* **2010**, *4*, 2009–2020.
- (30) Vogel, W.; Rosner, B.; Tesche, B. Structural investigations of gold (Au55) organometallic complexes by x-ray powder diffraction and transmission electron microscopy. *J. Phys. Chem.* **1993**, *97*, 11611–11616.
- (31) Rapoport, D. H.; Vogel, W.; Cölfen, H.; Schlögl, R. Ligand-Stabilized Metal Clusters: Reinvestigation of the Structure of "Au55[P(C6H5)3]12Cl6. *J. Phys. Chem. B* **1997**, *101*, 4175–4183.
- (32) Heiles, S.; Johnston, R. L. Global optimization of clusters using electronic structure methods. *Int. J. Quantum Chem.* **2013**, *113*, 2091–2109.
- (33) Jäger, M.; Schäfer, R.; Johnston, R. L. First principles global optimization of metal clusters and nanoalloys. *Advances in Physics: X* **2018**, *3*, S100009.
- (34) Baletto, F. Structural properties of sub-nanometer metallic clusters. *J. Phys.: Condens. Matter* **2019**, *31*, 113001.
- (35) Johansson, M. P.; Warnke, I.; Le, A.; Furche, F. At What Size Do Neutral Gold Clusters Turn Three-Dimensional? *J. Phys. Chem. C* **2014**, *118*, 29370–29377.
- (36) Kinaci, A.; Narayanan, B.; Sen, F. G.; Davis, M. J.; Gray, S. K.; Sankaranarayanan, S. K. R. S.; Chan, M. K. Y. Unraveling the Planar-Globular Transition in Gold Nanoclusters through Evolutionary Search. Sci. Rep. 2016, 6, 34974.
- (37) Bulusu, S.; Zeng, X. C. Structures and relative stability of neutral gold clusters: Aun (n = 15–19). *J. Chem. Phys.* **2006**, *125*, 154303.
- (38) Jiang, D.-e.; Walter, M. Au<sub>40</sub>: A large tetrahedral magic cluster. *Phys. Rev. B: Condens. Matter Mater. Phys.* **2011**, *84*, 193402.
- (39) Chaves, A. S.; Piotrowski, M. J.; Da Silva, J. L. F. Evolution of the structural, energetic, and electronic properties of the 3d, 4d, and 5d transition-metal clusters (30 TMn systems for n=2-15): a density functional theory investigation. *Phys. Chem. Chem. Phys.* **2017**, 19, 15484–15502.
- (40) Johansson, M. P.; Sundholm, D.; Vaara, J. Au32: A 24-Carat Golden Fullerene. *Angew. Chem., Int. Ed.* **2004**, *43*, 2678–2681.
- (41) Wang, J.; Jellinek, J.; Zhao, J.; Chen, Z.; King, R. B.; von Ragué Schleyer, P. Hollow Cages versus Space-Filling Structures for Medium-Sized Gold Clusters: The Spherical Aromaticity of the Au50 Cage. J. Phys. Chem. A 2005, 109, 9265–9269.
- (42) Pyykko, P. Relativistic effects in structural chemistry. Chem. Rev. 1988, 88, 563-594.
- (43) Schwerdtfeger, P.; Dolg, M.; Schwarz, W. H. E.; Bowmaker, G. A.; Boyd, P. D. W. Relativistic effects in gold chemistry. I. Diatomic gold compounds. *J. Chem. Phys.* **1989**, *91*, 1762–1774.
- (44) Tarrat, N.; Rapacioli, M.; Cuny, J.; Morillo, J.; Heully, J.-L.; Spiegelman, F. Global optimization of neutral and charged 20- and 55-atom silver and gold clusters at the DFTB level. *Comput. Theor. Chem.* **2017**, *1107*, 102–114.

- (45) Tarrat, N.; Rapacioli, M.; Spiegelman, F. Au147 nanoparticles: Ordered or amorphous? *J. Chem. Phys.* **2018**, *148*, 204–308.
- (46) Narayanan, B.; Kinaci, A.; Sen, F. G.; Davis, M. J.; Gray, S. K.; Chan, M. K. Y.; Sankaranarayanan, S. K. R. S. Describing the Diverse Geometries of Gold from Nanoclusters to Bulk——A First-Principles-Based Hybrid Bond-Order Potential. *J. Phys. Chem. C* **2016**, *120*, 13787—13800.
- (47) Doye, J. P.K.; Wales, D. J. Global minima for transition metal clusters described by Sutton—Chen potentials. *New J. Chem.* **1998**, 22, 733—744.
- (48) Wu, X.; Dong, Y. J. Geometrical structures and energetics of gold clusters from Au13 to Au300. Struct. Chem. 2015, 26, 393-400.
- (49) Boes, J. R.; Groenenboom, M. C.; Keith, J. A.; Kitchin, J. R. Neural network and ReaxFF comparison for Au properties. *Int. J. Quantum Chem.* **2016**, *116*, 979–987.
- (50) Behler, J.; Parrinello, M. Generalized Neural-Network Representation of High-Dimensional Potential-Energy Surfaces. *Phys. Rev. Lett.* **2007**, *98*, 146401.
- (51) Bernstein, N.; Csányi, G.; Deringer, V. L. De novo exploration and self-guided learning of potential-energy surfaces. *npj Comput. Mater.* **2019**, 5, DOI: 10.1038/s41524-019-0236-6.
- (52) Chiriki, S.; Jindal, S.; Bulusu, S. S. Neural network potentials for dynamics and thermodynamics of gold nanoparticles. *J. Chem. Phys.* **2017**, *146*, 084314.
- (53) Ouyang, R.; Xie, Y.; Jiang, D.-e. Global minimization of gold clusters by combining neural network potentials and the basin-hopping method. *Nanoscale* **2015**, *7*, 14817–14821.
- (54) Jindal, S.; Chiriki, S.; Bulusu, S. S. Spherical harmonics based descriptor for neural network potentials: Structure and dynamics of Au147 nanocluster. *J. Chem. Phys.* **2017**, *146*, 204301.
- (55) Hajinazar, S.; Sandoval, E. D.; Cullo, A. J.; Kolmogorov, A. N. Multitribe evolutionary search for stable Cu–Pd–Ag nanoparticles using neural network models. *Phys. Chem. Chem. Phys.* **2019**, *21*, 8729–8742.
- (56) Garzón, I. L.; Reyes-Nava, J. A.; Rodríguez-Hernández, J. I.; Sigal, I.; Beltrán, M. R.; Michaelian, K. Chirality in bare and passivated gold nanoclusters. *Phys. Rev. B: Condens. Matter Mater. Phys.* **2002**, *66*, 073403.
- (57) Wang, S.-Y.; Yu, J.-Z.; Mizuseki, H.; Yan, J.-A.; Kawazoe, Y.; Wang, C.-Y. First-principles study of the electronic structures of icosahedral TiN(N=13,19,43,55) clusters. *J. Chem. Phys.* **2004**, *120*, 8463-8468.
- (58) Erickson, J. D.; Mednikov, E. G.; Ivanov, S. A.; Dahl, L. F. Isolation and Structural Characterization of a Mackay 55-Metal-Atom Two-Shell Icosahedron of Pseudo-Ih Symmetry,  $Pd5SL12(\mu3-CO)20$  (L = PR3, R = Isopropyl): Comparative Analysis with Interior Two-Shell Icosahedral Geometries in Capped Three-Shell Pd145, Pt-Centered Four-Shell Pd-Pt M165, and Four-Shell Au133 Nanoclusters. *J. Am. Chem. Soc.* **2016**, 138, 1502–1505.
- (59) Wu, X.; Chen, S.; Sun, Y.; Chen, Y. Geometrical structures of gold clusters on Gupta and Sutton-Chen potentials. *Comput. Theor. Chem.* **2012**, *1002*, 43–48.
- (60) Kresse, G.; Hafner, J. Ab initio molecular dynamics for liquid metals. *Phys. Rev. B: Condens. Matter Mater. Phys.* **1993**, 47, 558–561.
- (61) Kresse, G.; Hafner, J. Ab initio molecular-dynamics simulation of the liquid-metal—amorphous-semiconductor transition in germanium. *Phys. Rev. B: Condens. Matter Mater. Phys.* **1994**, 49, 14251—14269.
- (62) Kresse, G.; Furthmüller, J. Efficiency of ab-initio total energy calculations for metals and semiconductors using a plane-wave basis set. *Comput. Mater. Sci.* **1996**, *6*, 15–50.
- (63) Kresse, G.; Furthmüller, J. Efficient iterative schemes for ab initio total-energy calculations using a plane-wave basis set. *Phys. Rev. B: Condens. Matter Mater. Phys.* **1996**, *54*, 11169–11186.
- (64) Perdew, J. P.; Burke, K.; Ernzerhof, M. Generalized Gradient Approximation Made Simple. *Phys. Rev. Lett.* **1996**, *77*, 3865–3868.
- (65) Langreth, D. C.; Mehl, M. J. Beyond the local-density approximation in calculations of ground-state electronic properties. *Phys. Rev. B: Condens. Matter Mater. Phys.* 1983, 28, 1809–1834.

- (66) Blöchl, P. E. Projector augmented-wave method. *Phys. Rev. B: Condens. Matter Mater. Phys.* **1994**, *50*, 17953–17979.
- (67) Monkhorst, H. J.; Pack, J. D. Special points for Brillouin-zone integrations. *Phys. Rev. B* **1976**, *13*, 5188–5192.
- (68) Kolmorgorov, A. N. Module for Ab Initio Structure Evolution; https://github.com/maise-guide/maise, 2019.
- (69) Hajinazar, S.; Shao, J.; Kolmogorov, A. N. Stratified construction of neural network based interatomic models for multicomponent materials. *Phys. Rev. B: Condens. Matter Mater. Phys.* **2017**, 95, 014114.
- (70) Gupta, R. P. Lattice relaxation at a metal surface. *Phys. Rev. B: Condens. Matter Mater. Phys.* **1981**, 23, 6265–6270.
- (71) Rosato, V.; Guillope, M.; Legrand, B. Thermodynamical and structural properties of f.c.c. transition metals using a simple tight-binding model. *Philos. Mag. A* **1989**, *59*, 321–336.
- (72) Baletto, F.; Mottet, C.; Ferrando, R. Growth simulations of silver shells on copper and palladium nanoclusters. *Phys. Rev. B: Condens. Matter Mater. Phys.* **2002**, *66*, 155420.
- (73) Cleri, F.; Rosato, V. Tight-binding potentials for transition metals and alloys. *Phys. Rev. B: Condens. Matter Mater. Phys.* **1993**, 48, 22–33
- (74) Rossi, G.; Schiappelli, G.; Ferrando, R. Formation pathways and energetic stability of icosahedral Ag shellCocore nanoclusters. *J. Comput. Theor. Nanosci.* **2009**, *6*, 841–848.
- (75) Wu, X.; Dong, Y. Theoretical studies of structures and energies of Pd, Au-Pd, and Au-Pd-Pt clusters. *New J. Chem.* **2014**, *38*, 4893–4900.
- (76) Plimpton, S. Fast Parallel Algorithms for Short-Range Molecular Dynamics. *J. Comput. Phys.* **1995**, *117*, 1–19.
- (77) Olsson, P. A. T. Transverse resonant properties of strained gold nanowires. *J. Appl. Phys.* **2010**, *108*, 034318.
- (78) Wales, D. J.; Doye, J. P. K. Global Optimization by Basin-Hopping and the Lowest Energy Structures of Lennard-Jones Clusters Containing up to 110 Atoms. J. Phys. Chem. A 1997, 101, 5111–5116.
- (79) Schönborn, S. E.; Goedecker, S.; Roy, S.; Oganov, A. R. The performance of minima hopping and evolutionary algorithms for cluster structure prediction. *J. Chem. Phys.* **2009**, *130*, 144108.
- (80) Kennedy, J.; Eberhart, R. Particle swarm optimization. *Proceedings of ICNN'95 International Conference on Neural Networks* **1995**, 4, 1942–1948.
- (81) Shao, X.; Cheng, L.; Cai, W. A dynamic lattice searching method for fast optimization of Lennard–Jones clusters. *J. Comput. Chem.* **2004**, *25*, 1693–1698.
- (82) Mitchell, M. An Introduction to Genetic Algorithms; MIT Press: Cambridge, MA, 1998.
- (83) Barrón, C.; Gómez, S.; Romero, D.; Saavedra, A. A genetic algorithm for Lennard-Jones atomic clusters. *Applied Mathematics Letters* **1999**, *12*, 85–90.
- (84) Daven, D.; Tit, N.; Morris, J.; Ho, K. Structural optimization of Lennard-Jones clusters by a genetic algorithm. *Chem. Phys. Lett.* **1996**, 256, 195–200.
- (85) Woodley, S. M.; Sokol, A. A.; Catlow, C. R. A. Structure Prediction of Inorganic Nanoparticles with Predefined Architecture using a Genetic Algorithm. *Z. Anorg. Allg. Chem.* **2004**, *630*, 2343–2353.
- (86) Shah, S.; Kolmogorov, A. N. Stability and superconductivity of Ca-B phases at ambient and high pressure. *Phys. Rev. B: Condens. Matter Mater. Phys.* **2013**, 88, 014107.
- (87) Alfê, D. PHON: A program to calculate phonons using the small displacement method. *Comput. Phys. Commun.* **2009**, *180*, 2622–2633.
- (88) Pilati, T.; Forni, A. SYMMOL: a program to find the maximum symmetry group in an atom cluster, given a prefixed tolerance. *J. Appl. Crystallogr.* **1998**, *31*, 503–504.
- (89) Kelchner, C. L.; Plimpton, S. J.; Hamilton, J. C. Dislocation nucleation and defect structure during surface indentation. *Phys. Rev. B: Condens. Matter Mater. Phys.* **1998**, *58*, 11085–11088.

- (90) Stukowski, A. Visualization and analysis of atomistic simulation data with OVITO—the Open Visualization Tool. *Modell. Simul. Mater. Sci. Eng.* **2010**, *18*, 015012.
- (91) Svalova, A.; Stishenko, P. Distribution of Active Site Types on Au Nanoparticles with Different Structures: Study of Thermal Dependence. *Procedia Eng.* **2016**, *152*, *67*–72 Presented at Oil and Gas Engineering (OGE-2016), Omsk State Technical University, Russian Federation, 25–30 April 2016 (Supported by PJSC Gazprom Neft)...
- (92) Suchomel, P.; Kvitek, L.; Prucek, R.; Panacek, A.; Halder, A.; Vajda, S.; Zboril, R. Simple size-controlled synthesis of Au nanoparticles and their size-dependent catalytic activity. *Sci. Rep.* **2018**, *8*, 4589.
- (93) Huang, X.; Wu, H.; Liao, X.; Shi, B. One-step, size-controlled synthesis of gold nanoparticles at room temperature using plant tannin. *Green Chem.* **2010**, *12*, 395–399.
- (94) Mountrichas, G.; Pispas, S.; Kamitsos, E. I. Effect of Temperature on the Direct Synthesis of Gold Nanoparticles Mediated by Poly(dimethylaminoethyl methacrylate) Homopolymer. *J. Phys. Chem. C* **2014**, *118*, 22754–22759.
- (95) Abdullah, A.; Altaf, M.; Khan, H. I.; Khan, G. A.; Khan, W.; Ali, A.; Bhatti, A. S.; Khan, S. U.; Ahmed, W. Facile room temperature synthesis of multifunctional CTAB coated gold nanoparticles. *Chem. Phys.* **2018**, *510*, 30–36.
- (96) Zuo, Y.; Chen, C.; Li, X.; Deng, Z.; Chen, Y.; Behler, J.; Csányi, G.; Shapeev, A. V.; Thompson, A. P.; Wood, M. A.; Ong, S. P. A Performance and Cost Assessment of Machine Learning Interatomic Potentials. *arXiv:1906.08888* 2019.
- (97) Towns, J.; Cockerill, T.; Dahan, M.; Foster, I.; Gaither, K.; Grimshaw, A.; Hazlewood, V.; Lathrop, S.; Lifka, D.; Peterson, G. D.; Roskies, R.; Scott, J. R.; Wilkins-Diehr, N. XSEDE: Accelerating Scientific Discovery. *Comput. Sci. Eng.* **2014**, *16*, 62–74.
- (98) Note that the  $r^{(0)} = 4.073$  parameter in ref 18 needed rescaling by a factor of  $\sqrt{2}$ .
- (99) It is worth noting that NN58 was actually more stable than Chi58 by 2.9 meV/atom with the lower DFT cutoff of 250 eV used in the original study,<sup>52</sup> but the latter underwent significant structural changes once reoptimized with our DFT settings (see Table 2).